LIMITATIONS OF CORRELATION-BASED REDATUMING METHODS

D. F. Barrera, J. Schleicher, and J. van der Neut

email: *js@ime.unicamp.br,diegofernando84@gmail.com*

keywords: *redatuming, interferometry, reciprocity, direct wave, artifacts, correlation-based extrapolation*

ABSTRACT

Interferometric redatuming techniques can be used to relocate sources to positions where only receivers are available and have been used to move acquisition geometries to the ocean bottom or transform data between surface-seismic and vertical seismic profiles. Even if no receivers are available at the new datum, the acquisition system can be relocated to any datum in the subsurface to which the propagation of waves can be modeled with sufficient accuracy. By correlating the modeled wavefield with seismic surface data, one can carry the seismic acquisition geometry from the surface closer to geologic horizons of interest. Specifically, we show the derivation and approximation of the one-sided seismic interferometry equation for surface-data redatuming. Our numerical examples demonstrate that correlation-based single-boundary redatuming works perfectly in a homogeneous overburden. If the overburden is inhomogeneous, primary reflections from deeper interfaces are still repositioned with satisfactory accuracy. However, in this case artifacts are generated as a consequence of incorrectly redatumed overburden multiples. These artifacts get even worse if the complete wavefield is used instead of the direct wavefield. Therefore, we conclude that correlation-based interferometric redatuming of surface seismic data should always be applied using direct waves only, which can be approximated with sufficient quality if a smooth velocity model for the overburden is available.

INTRODUCTION

Seismic data redatuming is a classic technique in the repertoire of seismic processing. Its purpose is to simulate data as if acquired at a new datum, i.e., a different measurement surface (Berryhill, 1979, 1984), generally located closer to the target. The redatuming technique's principal applications are the correction of surface seismic data for the effects of acquisition at an irregular surface or of complex geological structures in the overburden such as low-velocity layers or strong lateral variations. The objective is to generate improved seismic data that are easier to process and better illuminate the target (Wapenaar et al., 1992).

The first redatuming procedures discussed in the literature relied on the Kirchhoff integral (Wiggins, 1984; Wapenaar, 1993) and nowadays include amplitude corrections (Tegtmeier et al., 2004; Pila et al., 2014). Another line of research is dedicated to wave-equation-based redatuming (Yilmaz and Lucas, 1986; Schneider et al., 1995). More information on redatuming can be found in Schuster and Zhou (2006).

In recent years there has been a growing interest to improve petroleum exploration and processing of seismic data using interferometric techniques. Seismic interferometry is a technique based on optical physics. It allows the use of parts of the information contained in the seismic data that are not taken into account in conventional processing. Its idea is to generate new seismic responses or virtual sources where only receivers were placed (Wapenaar et al., 2010). In seismic exploration, Claerbout (1968) showed that the Green's function for reflections recorded at the Earth's surface could be obtained by the autocorrelation of the data generated by buried sources in a 1D medium, while Scherbaum (1978), using information of microquakes, constructed geological structure based on the properties of the Green's functions.

Interferometric redatuming can be used to relocate sources to positions where only receivers are available and allows to carry the seismic acquisitions from the surface to geologic horizons of interest. Different interferometric redatuming techniques have been studied by various authors. In a line of investigation most related to the present work, Curtis and Halliday (2010) present a method to construct unified representation theorems that combine the correlation and convolution types. According to their work, these combined theorems are more general than the separate ones. Moreover, they allow to derive a new form of source-receiver interferometry. Based on the derivations of Curtis and Halliday (2010), Poliannikov (2011) presents a interferometric redatuming method for recovering reflections that are missing in the virtual gather because of illumination problems. Comparing his results with those from the more classic form of interferometry, he concludes that the redatumed wavefield retrieved by the new procedure is more complete, because it includes the reflections from the overburden inhomogeneities in the redatumed data, allowing for imaging from below.

In this paper we discuss the use of the direct wave versus the full wave train in correlation-based interferometric redatuming. We derive the general correlation-based interferometric equation, which we approximate to a practically applicable form for surface-seismic data using the high-frequency WKBJ approximation. By means of numerical examples, we discuss the advantages and limitations of correlation-based interferometric redatuming, particularly the quality of the recovered physical events and the origins of the generated nonphysical events. We demonstrate that even if the inhomogeneous overburden above the datum is fully known, using only the direct wave for redatuming is advantageous over using the full wave train, because the latter generates much more artifacts. Finally, we show that the negative-time part of the redatumed data amounts to illumination from below of the datum overburden, in this way separating the reflections from above and below the datum.

METHOD

In this section we describe the basic theory of interferometry for acoustic media with density variation following the lines of Wapenaar et al. (2010), but using the notation of Bleistein et al. (2001). We start at the Helmholtz equation for variable-density media, which can be written as follows

$$\mathcal{L}\hat{\psi}(x,\omega) = \rho(x)\nabla\cdot\left[\frac{1}{\rho(x)}\nabla\hat{\psi}(x,\omega)\right] + \frac{\omega^2}{v^2(x)}\hat{\psi}(x,\omega) = -\hat{F}(x,\omega)\ . \tag{1}$$

Here, $\mathcal{L}$ is the Helmholtz operator with $\rho(x)$ denoting the variable density, $\hat{\psi}(x,\omega)$ the pressure field, ω the angular frequency, and $v(x)$ the wave velocity. Finally, $F(x,\omega)$ is a source term.

In the particular case of a temporal and spatial point source at position x_A, i.e., when the source term $F(x,\omega)$ is given by a delta function $\delta(x-x_A)$, the pressure field is represented by the Green's function $\hat{G}(x,\omega;x_A)$, so that the Helmholtz equation reads

$$\mathcal{L}\hat{G}(x,\omega,x_A) = \rho(x)\nabla\cdot\left[\frac{1}{\rho(x)}\nabla\hat{G}(x,\omega;x_A)\right] + \frac{\omega^2}{v^2(x)}\hat{G}(x,\omega;x_A) = -\delta(x-x_A). \tag{2}$$

The basis for all seismic interferometry is Gauss' theorem, which relates an integral over a closed surface ∂E of an arbitrary vector field to an integral over the enclosed volume E of the divergence of the vector field. Choosing the vector field appropriately, this theorem can be written as (Green, 1828)

$$\begin{aligned}\oiint_{\partial E}\frac{1}{\rho(x)}(\hat{\psi}\nabla\hat{G}-\hat{G}\nabla\hat{\psi})\cdot\hat{n}dS &= \iiint_E \nabla\cdot\left(\frac{1}{\rho(x)}\hat{\psi}\nabla\hat{G}-\frac{1}{\rho(x)}\hat{G}\nabla\hat{\psi}\right)dV \\ &= \iiint_E\left[\hat{\psi}\nabla\cdot\left(\frac{1}{\rho(x)}\nabla\hat{G}\right)-\hat{G}\nabla\cdot\left(\frac{1}{\rho(x)}\nabla\hat{\psi}\right)\right]dV,\end{aligned} \tag{3}$$

where $\hat{n}$ is the unit vector normal to the surface ∂E pointing into the outward direction of the volume E.

Interferometry

Let us now review the basic interferometry equation (see, e.g., Wapenaar et al., 2010). We consider the case where we have a closed surface with receivers located on it. Inside the enclosed volume, we have two

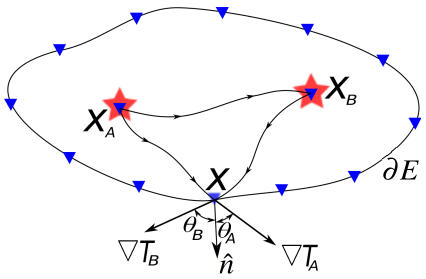

Figure 1: Sketch of two sources at positions x_A and x_B inside a volume E with receivers along the closed surface ∂E of E. Indicated at position x are the propagation directions of the incoming waves from x_A and x_B, and their angles θ_A and θ_B with respect to the unit normal vector $\hat{n}$ to the surface.

sources located in positions x_A and x_B (see Figure 1).

We start from the complex conjugate of the Helmholtz equation (1) with a point source at x_B. With the simplified notation $G_B^* = \hat{G}^*(x, \omega; x_B)$, where the asterisk denotes the complex conjugate, the corresponding equation reads

$$\rho(x)\nabla \cdot \left[\frac{1}{\rho(x)}\nabla \hat{G}_B^*\right] + \frac{\omega^2}{v^2(x)}\hat{G}_B^* = -\delta(x - x_B). \tag{4}$$

Multiplying equations (2) and (4) by $\hat{G}_B^*$ and $\hat{G}_A = \hat{G}(x, \omega; x_A)$, respectively, and subtracting the results after division by $\rho(x)$, we find

$$\hat{G}_A \nabla \cdot \left(\frac{1}{\rho(x)}\nabla \hat{G}_B^*\right) - \hat{G}_B^* \nabla \cdot \left(\frac{1}{\rho(x)}\nabla \hat{G}_A\right) = \frac{1}{\rho(x)}\left(\delta_A \hat{G}_B^* - \delta_B \hat{G}_A\right). \tag{5}$$

Integration over an arbitrary volume E, application of Green's version of Gauss' theorem (3), and consideration of reciprocity leads to

$$\oiint_{\partial E} \frac{1}{\rho(x)}\left(\hat{G}_A \nabla \hat{G}_B^* - \hat{G}_B^* \nabla \hat{G}_A\right) \cdot \hat{n} dS = \frac{-2i}{\rho(x_B)} \mathrm{Im}\left[\hat{G}(x_B, \omega; x_A)\right]. \tag{6}$$

This is the fundamental relationship for all interferometry techniques, because it proves that the (imaginary part of the) Green's function for the propagation from x_A to x_B can be obtained with information about the wavefield propagating from x_A and from x_B to (all) receivers on the closed surface. This is possible only if x_A and x_B are located inside the surface ∂E. Note that the form of equation (6) differs from the one of Wapenaar and Fokkema (2006) because of the different normalization of the Green's function.

Green's function approximation

While equation (6) is exact, it is generally not directly applicable in real situations, because it is extremely rare that data on closed surfaces are available. Moreover, the Green's functions' gradients generally are unknown. Therefore, the quantities in equation (6) need to be approximated by practically available data. For the following considerations, we refer again to Figure 1.

In the high-frequency situation, we can replace the Green's functions by their WKBJ approximations,

$$\hat{G}(x, \omega; x_s) \approx L(x; x_s) \exp\left[-i\omega T(x; x_s)\right]. \tag{7}$$

There, T is the traveltime from x_s to x which satisfies the eikonal equation $\|\nabla T(x; x_s)\|^2 = \frac{1}{v^2(x)}$ and $L(x; x_s)$ is the amplitude, mainly determined by geometrical spreading but also including all other factors affecting seismic amplitudes. Still in high-frequency approximation, the gradients of the Green's functions $\hat{G}_A$ and $\hat{G}_B$ can be approximated according to

$$\nabla \hat{G}(x, \omega; x_s) \approx -i\omega \hat{G}(x, \omega; x_s) \nabla T. \tag{8}$$

Upon substitution of this approximation in equation 6, the traveltime gradients of both Green's functions are multiplied with the surface normal. These products can be geometrically interpreted as $\nabla T \cdot \hat{n} =$

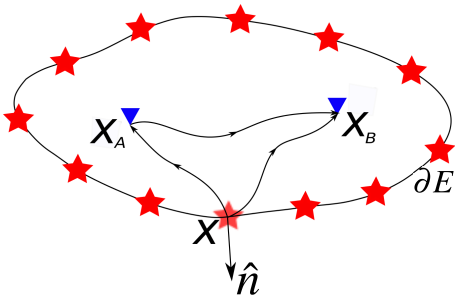

Figure 2: Sketch of two receivers at positions x_A and x_B inside an arbitrary volume E and sources along the closed surface ∂E of E.

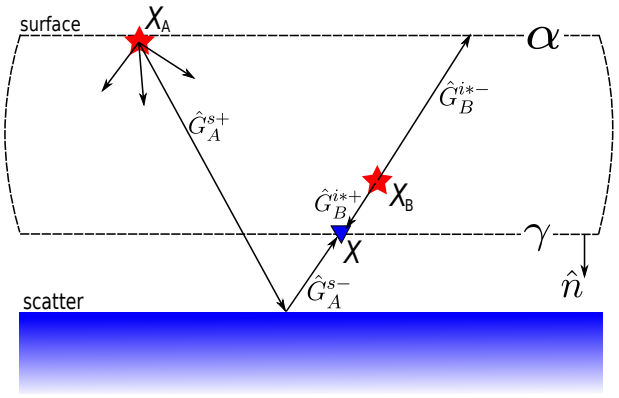

Figure 3: Sketch of the surface parts α and γ of ∂E including points x_A and x_B. The scattering surface below γ is supposed to contain the unknown part of the medium.

$\cos\theta/v(x)$, where θ is the incidence angle of the wavefield under consideration at the surface ∂E. Thus, under definition of the obliquity factor $\Theta(x; x_A, x_B) = (\cos\theta_A + \cos\theta_B)/2v(x)$, we can approximately represent equation (6) as

$$-\omega\rho(x_B)\oiint_{\partial E}\frac{1}{\rho(x)}\hat{G}_A\hat{G}_B^*\Theta(x; x_A, x_B)dS \approx \mathrm{Im}\left[\hat{G}(x_B, \omega; x_A)\right]. \tag{9}$$

If the surface is sufficiently far away from the points x_A and x_B, the angles θ_A and θ_B between the ray paths and the surface normal approximately vanish, so that $\Theta \approx \frac{1}{v(x)}$. Thus, in far-field approximation, we can write

$$-\omega\rho(x_B)\oiint_{\partial E}\frac{1}{\rho(x)v(x)}\hat{G}_A\hat{G}_B^*dS \approx \mathrm{Im}\left[\hat{G}(x_B, \omega; x_A)\right]. \tag{10}$$

Equation (10) shows that the situation of Figure 1 can be exchanged for one where instead of sources inside the volume, there are receivers, and instead of receivers at the surface, there are sources. This is the reciprocity principle (see Figure 2).

Direct-wave redatuming

We now want to make use of equation (10) for redatuming of surface-seismic data. For this purpose, we suppose that the medium inside the closed surface ∂E in Figure 1 is known. We then consider the situation in Figure 3. We understand the surface ∂E as divided into two parts α and γ. The surface α contains all sources and receivers of a conventional seismic array, and γ is a surface part that is needed to close it.

We suppose that available seismic data have been acquired at receivers distributed along the seismic array at α for sources at points x_A (also at α). We want to simulate seismic data at the same receivers for sources at points x_B in the subsurface inside the closed surface ∂E formed by its parts α and β. With the known velocity model for the medium between surface parts α and γ, the direct wave from all points x_B on the datum to all points x_A on α can be estimated by seismic modeling. We will show in this section that cross-correlation of this modeled direct waves with the seismic surface data allows to approximately redatum the acquisition array (sources and receivers) to reference datum scatter.

The total Green's function for the wavefield at surface α can then be decomposed as $\hat{G} = \hat{G}^i + \hat{G}^s$ (Bleistein et al., 2001), where $\hat{G}^i$ is the solution of the wave equation in a known reference medium and $\hat{G}^s$ is the difference to the complete solution in the true medium. For a point source at x_A, $\hat{G}_A^i = \hat{G}^i(x, \omega; x_A)$ must satisfy

$$\mathcal{L}_0\hat{G}_A^i = -\delta(x - x_A), \tag{11}$$

where $\mathcal{L}_0$ is the Helmholtz operator for the reference medium, involving the known density ρ_0 and velocity v_0 instead of the unknown ones ρ and v.

The scattered field $\hat{G}^s_A = \hat{G}^s(x, \omega; x_A)$ must satisfy a perturbed wave equation that can be written as

$$\mathcal{L}_0 \hat{G}^s_A = -\mathcal{V}(x) \left[\hat{G}^i_A + \hat{G}^s_A \right], \tag{12}$$

where $\mathcal{V}(x) = \mathcal{L} - \mathcal{L}_0$ is the difference between the perturbed and unperturbed Helmholtz operators, called the perturbation operator or scattering potential (Rodberg and Thaler, 1967).

In other words, the differences between the reference and true media are responsible for the existence of the scattering potential $\mathcal{V}$ and thus for the existence of the scattered wavefield $\hat{G}^s$. We assume that the region where the true medium is not known, i.e., where the perturbations between the reference medium and the true medium are located, is the scattering body (indicated as blue region in Figure 3) outside ∂E.

Using equations (11) and (12), we can set up an equation similar to equation (5). For this purpose, we multiply equation (12) with G^{i*}_B and the complex conjugate of equation (11) for a point source at x_B with G^s_A. Subtracting the results, we arrive at

$$\hat{G}^s_A \nabla \cdot \left(\frac{1}{\rho_0(x)} \nabla \hat{G}^{i*}_B \right) - \hat{G}^{i*}_B \nabla \cdot \left(\frac{1}{\rho_0(x)} \nabla \hat{G}^s_A \right) = \frac{1}{\rho_0(x)} \left(\hat{G}^{i*}_B \mathcal{V} \hat{G}_A - \delta_B \hat{G}^s_A \right). \tag{13}$$

After integration over a volume E containing x_B and application of Green's theorem, this yields

$$\oiint_{\alpha+\gamma} \frac{1}{\rho_0(x)} \left(\hat{G}^s_A \nabla \hat{G}^{i*}_B - \hat{G}^{i*}_B \nabla \hat{G}^s_A \right) \cdot \hat{n} dS = \iiint_E \frac{\hat{G}^{i*}_B \mathcal{V} \hat{G}_A}{\rho_0(x)} dV - \frac{\hat{G}^s_{BA}}{\rho_0(x_B)}, \tag{14}$$

where $\hat{G}^s_{BA} = \hat{G}^s(x_B, \omega; x_A)$. As indicated before, we have written the closed surface ∂E as a sum of its two parts, where α represents the portion where seismic data are available and γ the remaining portion.

Since we suppose the datum overburden to be known, we can choose the volume E such that $\mathcal{V} = \mathcal{L} - \mathcal{L}_0 = 0$ inside E (see Figure 3). Thus, the volume integral in equation (14) vanishes (Vasconcelos et al., 2009) . After high-frequency approximations analogous to equations (7) and (8), equation (14) therefore allows to approximately calculate the scattered field at x_B as

$$\hat{G}^s(x_B, \omega; x_A) \approx -2i\omega \iint_\alpha \int \frac{\rho_0(x_B)}{\rho_0(x)} \hat{G}^s_A \hat{G}^{i*}_B \Theta(x; x_A, x_B) dS. \tag{15}$$

In our numerical experiments, we approximated the obliquity factor $\Theta(x; x_A, x_B)$ as $\Theta(x; x_A, x_B) \approx 1/v$. Here, we have neglected the contribution of the surface integral along γ in equation (14). According to Wapenaar and Berkhout (1989), this an acceptable approximation if there are no scatterers inside ∂E. We studied the consequences of this approximation in our numerical experiments reported below.

Equation (15) states that it is possible to redatum surface data by means of interferometry using wave modeling. This equation allows to obtain the Green's function at x_B for a point source at x_A by cross-correlation of the modeled wave in x_B with the acquired wavefield in x_A. In our numerical tests, we will study the effect of using the direct wave only instead of the full reference wavefield $\hat{g}^i_B$ to study how that affects the quality of the results.

NUMERICAL EXAMPLES

We numerically validated the interferometric redatuming equation (15), and we tested its limitations due to the use of the direct wave instead of the full reference wavefield, by applying it to synthetic data from simple models.

Datum below a homogeneous layer

Our first test used a horizontally-layered velocity model with a width of 8 km and a depth of 3 km containing velocities between 1.8 km/s and 2.5 km/s (Figure 5). The datum is located 500 m below the surface within the first homogeneous layer with velocity 1.8 km/s. This experiment represents the ideal situation, where the reference wavefield consists only of a direct wave.

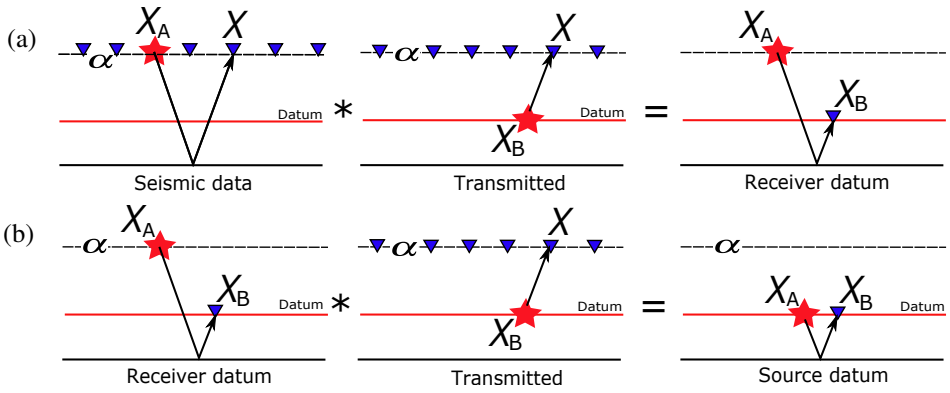

Figure 4: Sketch that shows the redatuming of a seismic survey to a new datum $\partial\Sigma$ in two steps: (a) sources and (b) receivers.

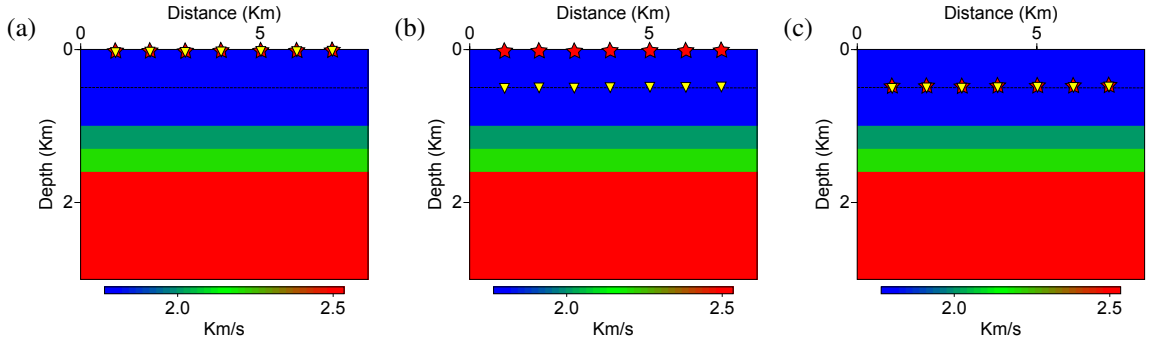

Figure 5: Modeling seismic data considering: (a) array of sources and receivers at the surface, (b) array of shots at the surface and receivers at 500 m depth and (c) both arrays positioned at 500 m depth.

By a single application of equation (15), only the receivers are repositioned from x to x_B, while the sources are still kept at their original positions x_A. To redatum the complete survey, equation (15) must be applied twice, using the reciprocity principle. After the first step, redatuming the receivers, the data need to be resorted into common-receiver gathers in order to redatum the sources using the same equation (15) with the roles of sources and receivers interchanged (see Figure 4).

Data We simulated synthetic data with a marine acquisition geometry considering three situations: (1) Shots and receivers are located at the surface (Figure 5a). These are the data to be redatumed. (2) Shots are located at the surface and receivers at 500 m depth (Figure 5b) and (3) shots and receiver are located at 500 m depth (Figure 5c). The data of the latter two simulations are used for comparison to the redatuming results.

All three seismic arrays consisted of 201 sources spaced at 25 m, horizontally located between coordinates 1 km and 6 km, and the same number of receivers for each shot, located at the same horizontal positions (Figure 5). The wavelet used for the numerical modeling was a Ricker wavelet with 25 Hz peak frequency. For simplicity, we considered the density in all layers constant.

Redatuming The first step of redatuming the complete seismic array from the surface to the datum consisted of redatuming the receivers, i.e., transforming the configuration of Figure 5a into the geometry of Figure 5b. The second step of the complete redatuming of the full survey consists of repositioning the sources at depth, i.e., transforming the configuration of experiment shown in Figure 5b into the one shown in Figure 5c. For this purpose, we sort the data into common-receiver gathers. These can be redatumed using again equation (15) because of the reciprocity principle.

We used both datasets, the one obtained from redatuming the receivers and the one modeled at the datum, as an input to this second redatuming step. Figure 6 compares the results of this redatuming to

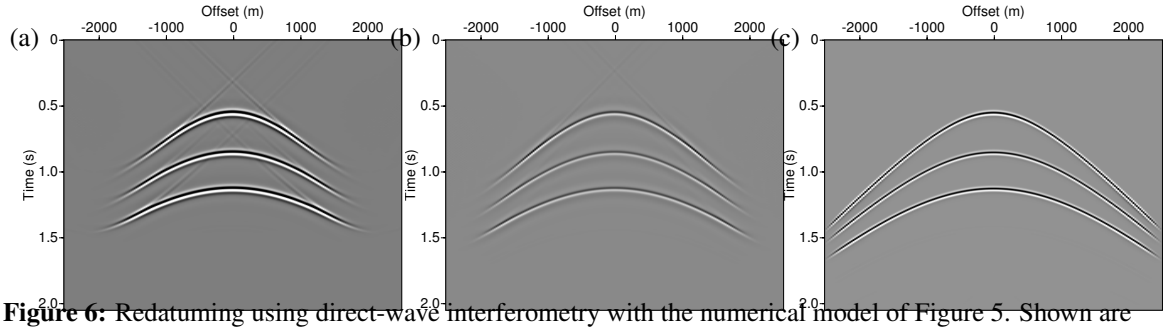

Figure 6: Redatuming using direct-wave interferometry with the numerical model of Figure 5. Shown are the data for sources and receivers at the datum, obtained from (a) source-receiver redatuming the surface data, (b) source-redatuming the data modeled with receivers at the datum, (c) modeling at the datum.

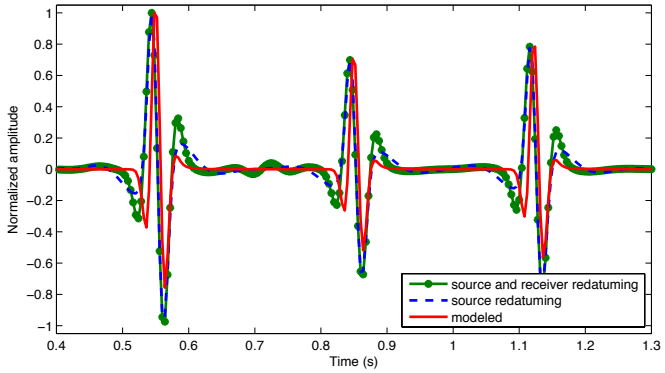

Figure 7: Comparison of the normalized central trace of the fully redatumed shot gather (dash-dotted green line) with the corresponding traces obtained from modeling (solid red line) and from redatuming the gather modeled with the receivers at the datum (dashed blue line).

the modeled data at the datum. We see that the positioning of the three reflections events in the two-step result (Figure 6a) matches those in the one-step result (Figure 6b) and the modeled data (Figure 6c) at the theoretical traveltimes.

The two-step redatuming of the surface data introduces some additional noise, particularly at the border of the events. These are boundary effects that result from the limited data aperture. These effects are restricted to the boundary zone and are of less importance if more input data are available. Moreover, they can be mitigated by using appropriate tapering filters.

For a more detailed analysis of the quality of the redatumed data, Figure 7 compares the normalized redatumed trace at the center of both the source and receiver arrays to the corresponding modeled one. As after receiver redatuming, all events are correctly positioned in time, and their relative amplitudes are correctly recovered. We observe again that the redatuming has caused a certain wavelet deformation and stretch, because we did not deconvolve the data with the source wavelet.

Datum below a high-velocity layer

In the second numerical experiment, we chose a model with a high-velocity layer (2.5 km/s) from 120 m to 400 m depth, between the original acquisition surface and the datum at 500 m depth. The lower part of the model is the same as before (Figure 8a).

Data In this situation, the reference wavefield includes the direct wave and later arrivals due to scattering in the high-velocity layer. To restrict the number of visible multiples, we did not use a free boundary at the top of the model. Our purpose is to see how these later arrivals affect the quality of the redatumed data.

Figure 8 shows the modeled synthetic data with labeled events and ray-path sketches, separated in primary reflections (Figure 8a) and the most prominent multiples (Figure 8b). The zero-offset times of

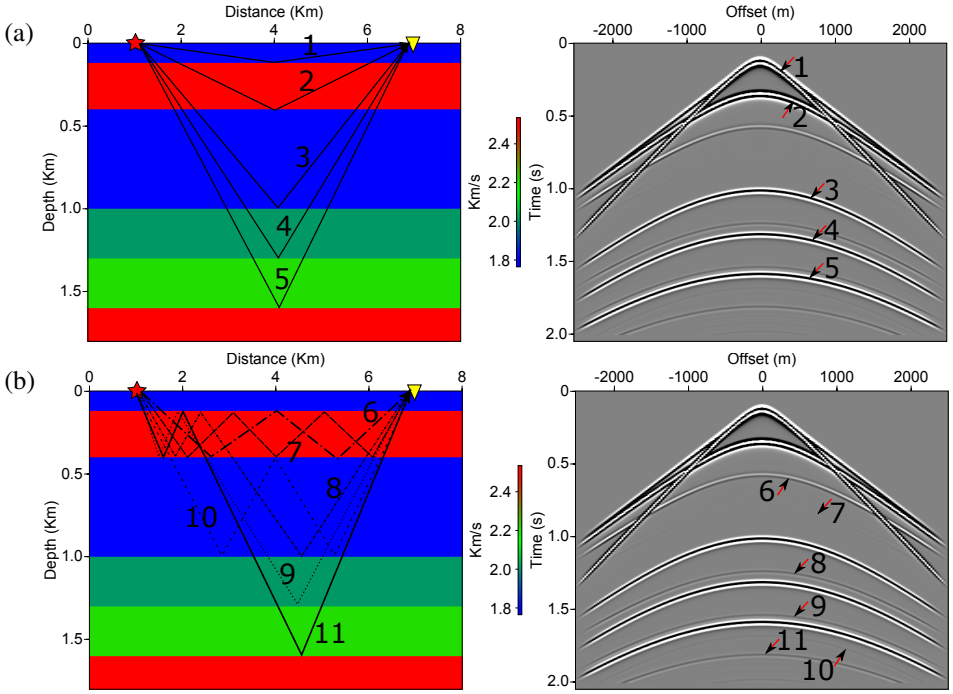

Figure 8: Seismic array on surface considering a inhomogeneous overburden, where we describe: (a) primary reflection events and (b) multiple events visible in the data.

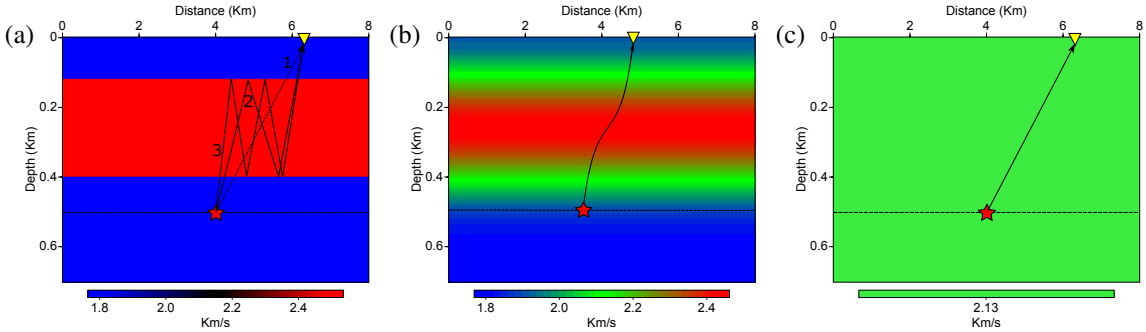

Figure 9: Models used for direct-wavefield modeling in the redatuming procedure. (a) Exact overburden. (b) Smoothed overburden. (c) Constant velocity from average slowness. Also shown are possible ray paths connecting sources at the datum to receivers at the surface.

the primary reflections are: $t_1 = 0.133$ s, $t_2 = 0.357$ s, $t_3 = 1.024$ s, $t_4 = 1.324$ s and $t_5 = 1.597$ s (Figure 8a). The strongest multiples are: Events 6 and 10 are the first multiples in the second and third layers with zero-offset times $t_6 = 0.581$ s and $t_{10} = 1.690$ s; events 8, 9, and 11 are peg-leg multiples with $t_8 = 1.248$ s, $t_9 = 1.548$ s, and $t_{11} = 1.820$ s; and event 7 is a second-order multiple in the second layer with $t_7 = 0.805$ s (Figure 8b). Other higher-order multiples are present in the data but their amplitudes are too small to be visible. Not labeled is the head wave, which is the first event at offsets larger than 250 m.

Redatuming The redatuming procedure is the same as detailed for the first example. Also as before, we modeled synthetic data for 201 sources and receivers, spaced at 25 m. For the direct-wave modeling in the redatuming process, we used three different background models, shown in Figure 9. The first model uses the exact velocity model in the region between the surface and the datum (Figure 9a). In the second test, we use a smoothed model (Figure 9b), and in the third test, we use a constant-velocity model with the correct average slowness (Figure 9c). Figure 9 also shows ray paths associated with the modeled events in these

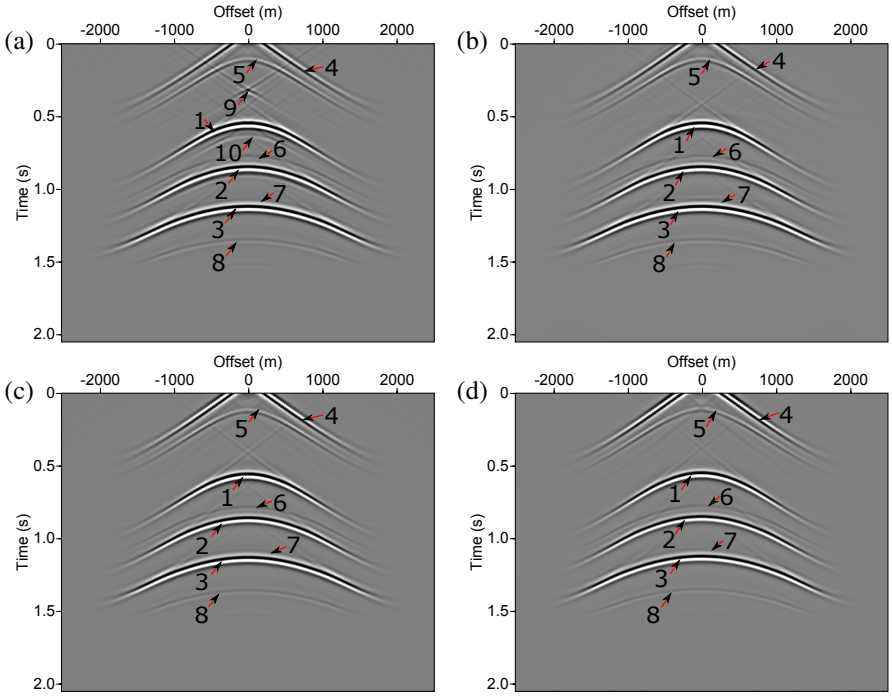

Figure 10: Result of redatuming with the (a) full wave train from the exact inhomogeneous overburden velocity model, (b) direct wave from the exact model, (c) direct wave from the smoothed model, and (d) direct wave from the constant-velocity model. The resulting redatumed events are labeled with numbers.

overburden models. With the exact model (Figure 9a), we carried out two experiments, one modeling the direct wave only by means of one-way wave propagation, and the other modeling the complete wave train.

The results of the cross-correlations between the data of Figure 8 and the different transmitted waves using the models of Figure 9 are shown in Figure 10. As a first observation, we notice that redatuming using the full wave train in the inhomogeneous overburden between the surface and the datum (Figure 10a) creates much more events then redatuming using the direct wave only (Figure 10b-d). A comparison with the desired result (Figure 6c) reveals that even the other results contain more events than they should. Moreover, we notice upon closer inspection that the kinematic behavior of the data redatumed using the constant-velocity model (Figure 10d) is slightly incorrect at non-zero offset.

The principal conclusion from this experiment is that it might not be convenient use equation (15) for redatuming in a strongly inhomogeneous overburden. As we can see in Figure 10, all ways of modeling the wavefield in the overburden produce unphysical events that should not be present in the redatumed data. In any case, using the direct wave only for redatuming is advantageous over using the full wave train, even if the overburden model is exactly known.

Event interpretation To explain all events present in the parts of Figure 10, we have labeled them. In the next set of figures, we will discuss the ray paths associated to all (physical and unphysical) events. In this way, we will be able to better understand the shortcomings of each of the tested modeling approaches.

The events labeled 1, 2, and 3 are the desired primary reflections from the deeper reflectors after redatuming. The corresponding ray paths associated with the original surface events, the two-step redatuming operators (representing the convolution of the two one-step operators), and the redatumed events are depicted in Figure 11.

Event 4 is a boundary effect of the redatuming of the primary reflection at the first interface in the overburden. Events 5, 6, 7, and 8 (see ray paths in Figure 12) are unphysical events resulting from redatuming the multiples with a first leg in the high-velocity layer (events 6, 8, 9, and 11 in Figure 8b) with the direct wave.

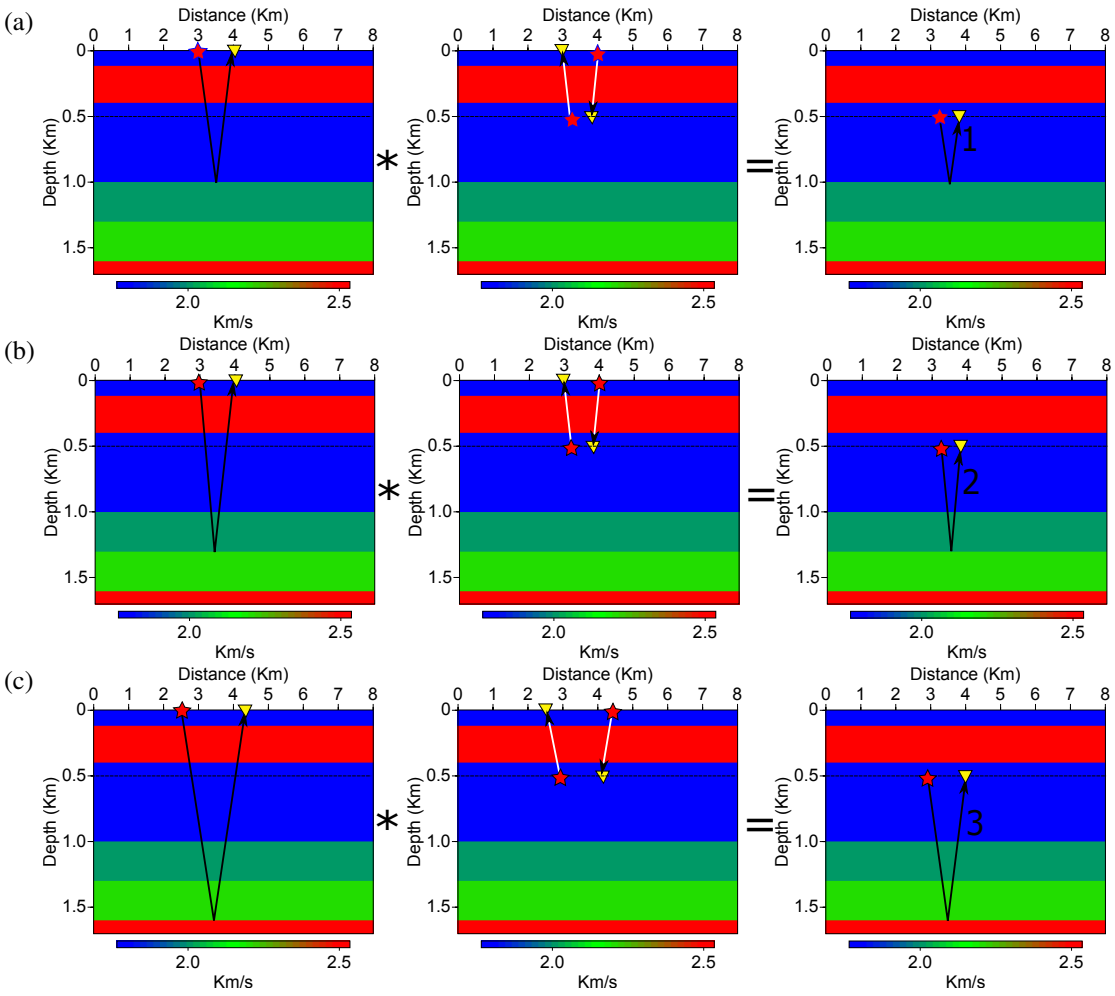

Figure 11: Ray paths for the surface events, cross-correlation operator, and redatuming response, for events 1, 2 and 3 of Figure 10.

Events 9 and 10 appear only in Figure 10a, because they are unphysical events caused by cross-correlation of the data primaries with multiples in the modeled wave train. Specifically, these events are obtained from redatuming the primaries of the 3rd and 4th reflectors (events 3 and 4 in Figure 8a) with the direct wave at the receiver side and with the first high-velocity-layer multiple at the source side or vice versa (see ray paths in Figure 13). A corresponding event generated from the primary at the deepest interface is present (but barely visible) immediately after event 2 in Figure 10a.

Finally, we can analyze the anti-causal part of the redatumed wavefield. Here, we restrict ourselves to the one obtained with the full wave train in the true overburden model (Figure 14. The other three results are similar, but do not contain the events obtained from cross-correlation with the multiples. It should be kept in mind that the desired part of the redatumed wavefield is its causal part.

Events 11 and 12 are the primary reflections from the two interfaces in the overburden. Since they are above the datum, they appear in the redatumed data at negative traveltimes. Also visible is initial part of the redatumed head wave (event 4 in Figure 10). Finally, events 13 and 14 are the events caused by redatuming these primaries with a direct wave and a multiple in the same way as explained for events 9 and 10 in Figure 10a. The ray paths associated with these events at negative traveltimes are depicted in Figure 15.

As graphically explained in Figure 15a and b, events 11 and 12 correspond to illumination of the overburden interfaces from below. This means that the negative-traveltime data in Figure 14 could be migrated (for example with the smooth velocity model in Figure 9b) to produce an image from below of

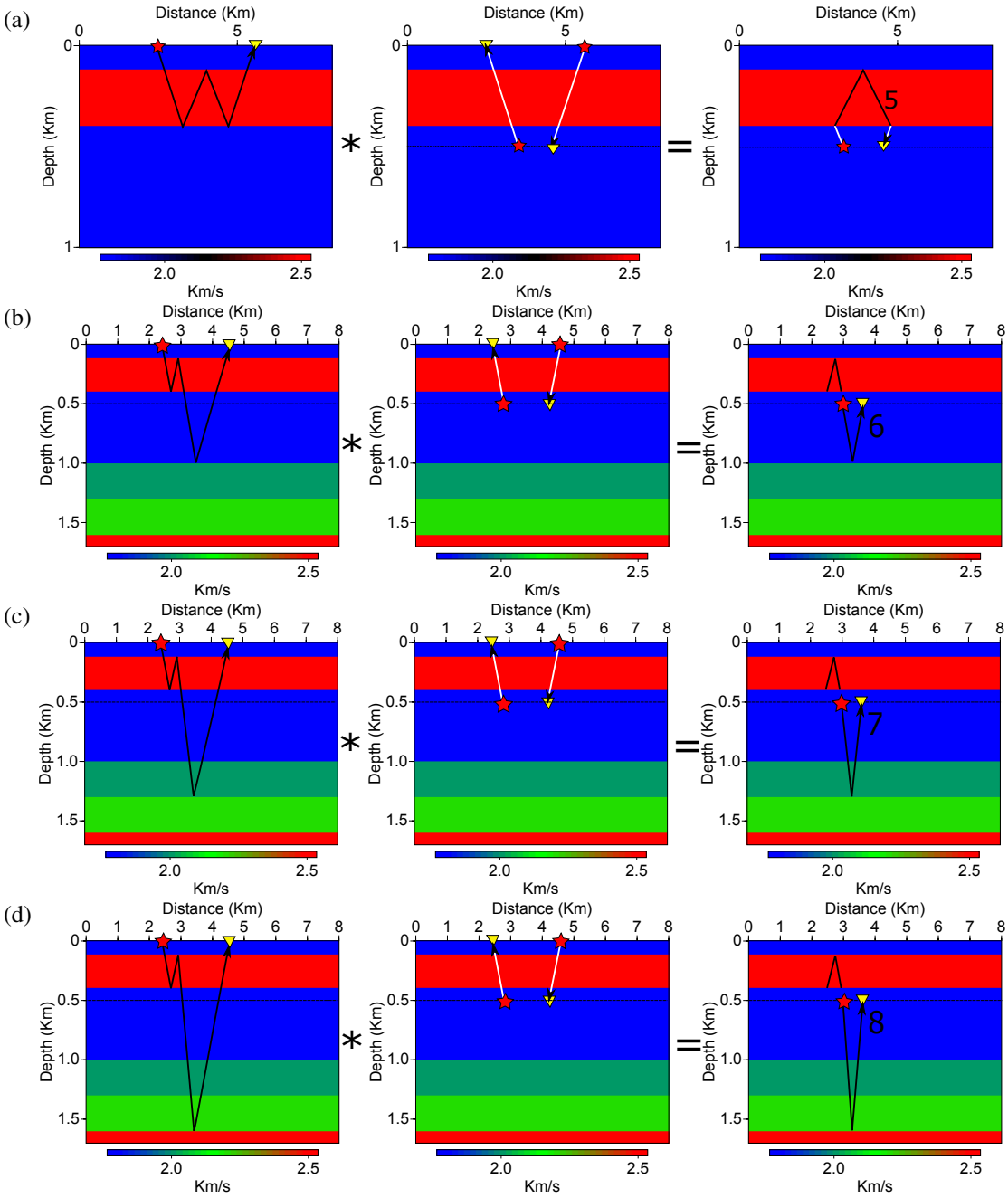

Figure 12: Ray paths for the surface events, cross-correlation operator, and redatuming response, for unphysical events 5, 6, 7, and 8 of Figure 10. Ray paths contributing negatively to the traveltimes are shown in white.

the overburden structures.

It is instructive to note that a similar type of Green's function retrieval from below has been proposed by Poliannikov (2011). He derived his results from source-receiver interferometry (Curtis and Halliday, 2010), which is based on a correlation-based closed-boundary representation. Hence, it suffers from similar artifacts as discussed in this paper. Single-sided representations for imaging from below (and from above) the overburden in arbitrarily heterogeneous media have also been derived from the multidimensional Marchenko equation (Wapenaar et al., 2014; Ravasi et al., 2016; Liu et al., 2016). Unlike the correlation-

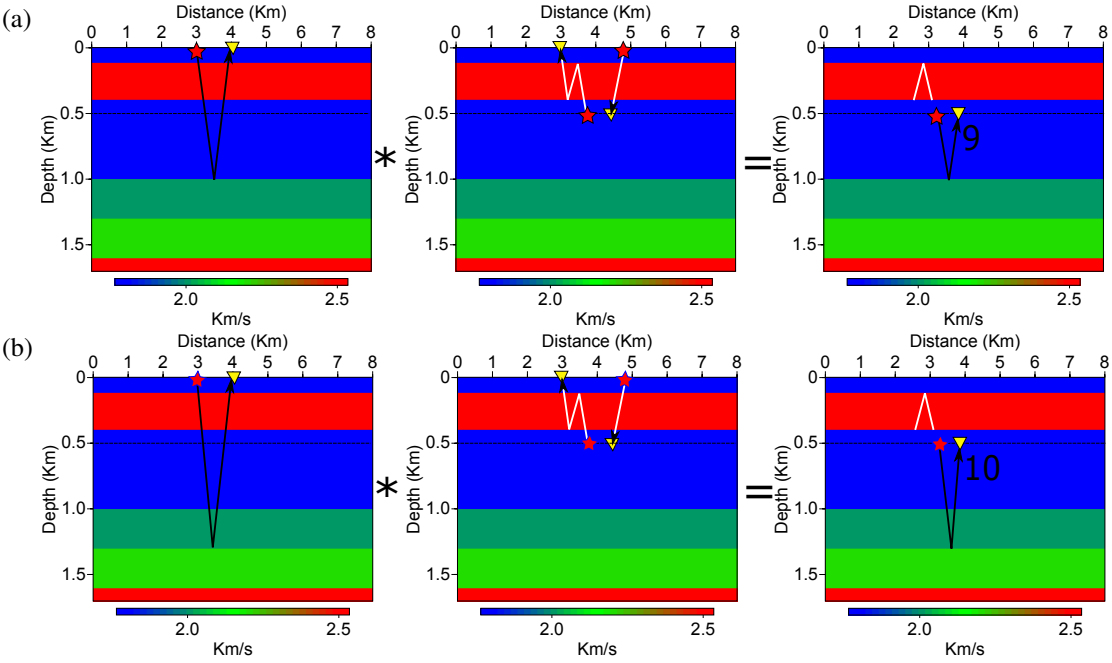

Figure 13: Ray paths for the surface events, cross-correlation operator, and redatuming response, for unphysical events 9 and 10 of Figure 10a. Ray paths contributing negatively to the traveltimes are shown in white.

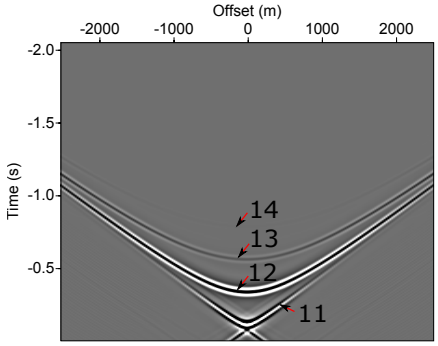

Figure 14: Anti-causal part of the redatuming result using the full wave train from the exact overburden velocity model. The labeled events are explained in the text.

based representations that are discussed in this paper, these representations do not suffer from artifacts caused by internal multiple reflections.

For a more detailed analysis of the redatuming results in Figure 10, we show in Figure 16 the normalized traces at offset 100 m of the redatumed data, obtained using the full wave train in the exact overburden and the direct wave in the exact, smoothed and constant-velocity models as compared to the data modeled at the datum. The three primary events are correctly positioned and their relative amplitudes are well preserved. In addition to these desired effects, we notice a number of events with smaller amplitudes. These are the unphysical events as discussed above. Note that the true internal multiples in the medium below the datum are of much smaller amplitude and cannot be seen at this scale. The traces obtained with the direct waves in the exact, smoothed, and average-velocity models are very similar to each other, with a very small kinematic error for the average-velocity model.

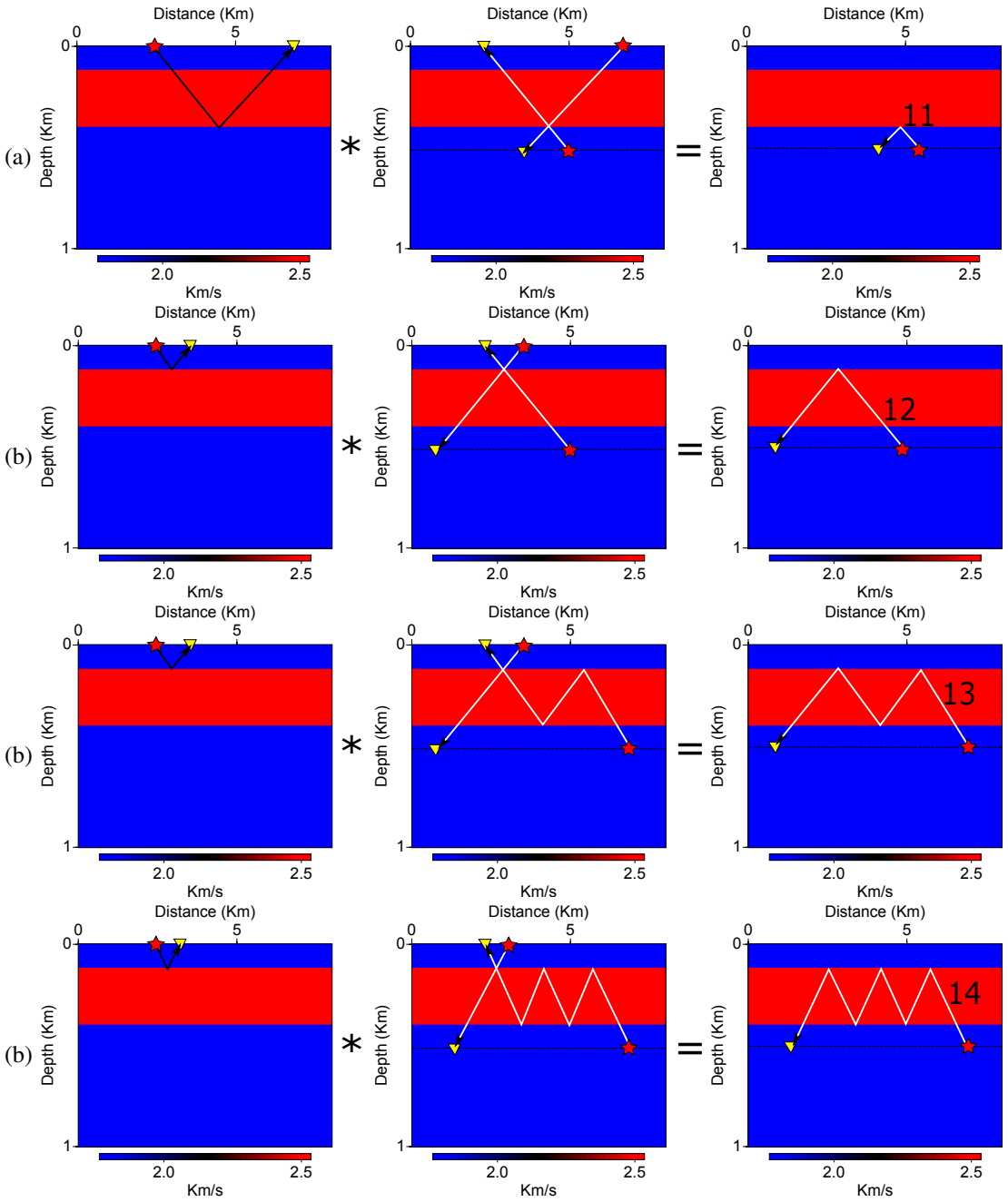

Figure 15: Ray paths for the surface events, cross-correlation operator, and redatuming response, for events 11, 12, 13, and 14 of Figure 14. Ray paths contributing negatively to the traveltimes are shown in white.

CONCLUSIONS

Interferometric redatuming is based on cross-correlating data at different receiver positions to construct data as if recorded using another source position. In this work, we have studied an interferometric redatuming method that uses the direct wavefield modeled in the known overburden of the new datum to redatum surface data. We have shown that a cross-correlation of the modeled direct wavefield with seismic surface data permits to relocate the acquisition system to any datum in the subsurface to which the propagation of direct waves can be modeled with sufficient accuracy.

The derivation starts from a convenient approximation of the seismic interferometry equation using

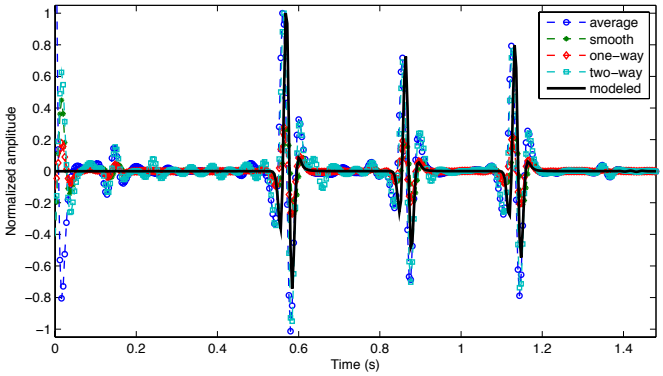

Figure 16: Comparison of the trace at 100 m offset obtained from redatuming using the full wave train in the exact overburden and the direct wave in the exact, smoothed and constant-velocity models.

Green's theorem on the Helmholtz equation. It proceeds to the general redatuming equation and the specific approximation discussing the correlation of acquired seismic data with modeled direct waves. As with conventional redatuming, also interferometric redatuming proceeds in two steps, independently relocating sources and receivers to the new datum.

To investigate the feasibility of the interferometric direct-wave redatuming, we have applied the method to synthetic surface data from a simple horizontally stratified model in order to construct redatumed data for sources and receivers at 500 m of depth. Our numerical example demonstrates that the redatumed reflections events are repositioned correctly and keep the correct amplitude proportions as compared to data obtained from seismic modeling at the datum level.

In our numerical experiments, we have also investigated the consequences of inhomogeneities in the overburden. If the medium between the surface and the datum is free of scatterers, the redatumed wavefield is only perturbed by boundary effects. However, if the overburden contains strong reflectors, unphysical events are created in the redatumed data. We have analyzed the kinematics of all visible reflections in the redatumed data to discuss their origins and distinguish physical from unphysical events. In this way, we have seen that the latter events are the consequences of incorrectly redatumed overburden multiples.

By means of numerical examples, we have discussed the advantages and limitations of correlation-based interferometric redatuming, particularly the quality of the recovered physical events and the origins of the generated nonphysical events. We demonstrate that even if the inhomogeneous overburden above the datum is fully known, using only the direct wave for redatuming is advantageous over using the full wave train. The latter procedure generates much more artifacts, because then, even the primaries can be incorrectly redatumed to give rise to yet more unphysical events in the redatumed data. This is a consequence of surface-seismic data allowing only for single-sided redatuming rather than redatuming from a closed boundary as required by the theory.

Finally, we have shown that the negative-time part of the redatumed data amounts to illumination from below of the datum overburden. This is particularly interesting in the light of redatuming being possible using the direct wave in a smoothed overburden. In this way, additional information about the overburden may become available after single-sided correlation-based direct-wave redatuming.

ACKNOWLEDGMENTS

We are grateful to the Brazilian agencies CNPq and FINEP, as well as Petrobras and the sponsors of the Wave Inversion Technology (WIT) Consortium for their support. The second author acknowledges a grant from the Santander Mobility Program.

REFERENCES

Berryhill, J. R. (1979). Wave-equation datuming. *Geophysics*, 44:1329–1344.

Berryhill, J. R. (1984). Wave equation datuming before stack. *Geophysics*, 49(11):2064–2067.

Bleistein, N., Cohen, J. K., and Jr., J. W. S. (2001). *Mathematics of Multidimensional Seismic Imaging, Migration, and Inversion*. Springer.

Claerbout, J. (1968). Synthesis of a layered medium from its acoustic transmission response. *Geophysics*, 33:264–269.

Curtis, A. and Halliday, D. (2010). Source-receiver wave field interferometry. *Physical Review*, 81:046601.

Green, G. (1828). *An essay on the application of mathematical analysis to the theories of electricity and magnetism*. Privately published.

Liu, Y., van der Neut, J., Arntsen, B., and Wapenaar, K. (2016). Combination of surface and borehole seismic data for robust target-oriented imaging. *Geophysical Journal International*, 205(2):758–775.

Pila, M. F., Schleicher, J., Novais, A., and Coimbra, T. A. (2014). True-amplitude single-stack redatuming. *Journal of Applied Geophysics*, 105:95–111.

Poliannikov, O. V. (2011). Retrieving reflections by source-receiver wavefield interferometry. *Geophysics*, 76:SA1–SA8.

Ravasi, M., Vasconcelos, I., Kritski, A., Curtis, A., da Costa Filho, C. A., and Meles, G. (2016). Target-oriented Marchenko imaging of a North Sea field. *Geophysical Journal International*, 205:99–104.

Rodberg, L. S. and Thaler, R. M. (1967). Introduction to the quantum theory of scattering. *Academic Press*.

Scherbaum, F. (1978). Seismic imaging of the site response using microearthquake recordings. Part II. Aplication to the Swabian Jura, southwest Germany, seismic network. *Bulletin of Seismological Society of America*, 77:1924–1944.

Schneider, W. A., Phillip, L. D., and Paal, E. F. (1995). Wave-equation velocity replacement of the low-velocity layer for overthrust-belt data. *Geophysics*, 60:573–580.

Schuster, G. and Zhou, M. (2006). A theoretical overview of model-based and correlation-based redatuming methods. *Geophysics*, 71:SI103–SI110.

Tegtmeier, S., Gisolf, A., and Verschuur, E. (2004). 3D sparse data Kirchhoff redatuming. *Geophysical Prospecting*, 52(6):509–521.

Vasconcelos, I., Snieder, R., and Douma, H. (2009). Representation theorems and Green's function retrieval for scattering in acoustic media. *Physcial Review*, 80.

Wapenaar, C. P. A. (1993). Kirchhoff-Helmholtz downward extrapolation in a layered medium with curved interfaces. *Geophys J. Int.*, 115:445–455.

Wapenaar, C. P. A. and Berkhout, A. J. (1989). *Elastic wave field extrapolation: redatuming of single- and multi-component seismic data*. Elsevier.

Wapenaar, C. P. A., Cox, H. L. H., and Berkhout, A. J. (1992). Elastic redatuming of multicomponent seismic data. *Geophysical Prospecting*, 40(04):465–482.

Wapenaar, K., Draganov, D., Snieder, R., Campman, X., and Verdel, A. (2010). Tutorial on seismic interferometry: Part 1 - basic principles and applications. *Geophysics*, 75:75A195–75A209.

Wapenaar, K. and Fokkema, J. (2006). Green's function representations for seismic interferometry. *Geophysics*, 71(4):SI33–SI46.

Wapenaar, K., Thorbecke, J., van der Neut, J., Broggini, F., Slob, E., and Snieder, R. (2014). Marchenko imaging. *Geophysics*, 79(3):WA39–WA57.

Wiggins, J. W. (1984). Kirchhoff integral extrapolation and migration of nonplanar data. *Geophysics*, 49:1239–1248.

Yilmaz, O. and Lucas, D. (1986). Prestack layer replacement. *Geophysics*, 51:1355–1369.